

# Antiarrhythmic effect linked to melatonin cardiorenal protection involves AT<sub>1</sub> reduction and Hsp70-VDR increase

Natalia Jorgelina Prado<sup>1</sup> | Mariana Casarotto<sup>1</sup> | Juan Pablo Calvo<sup>1</sup> |  
Luciana Mazzei<sup>1</sup> | Amira Zulma Ponce Zumino<sup>1,2</sup> | Isabel Mercedes García<sup>1</sup> |  
Fernando Darío Cuello-Carrión<sup>1</sup> | Miguel Walter Fornés<sup>3</sup> | León Ferder<sup>4</sup> |  
Emiliano Raúl Diez<sup>1,2</sup>  | Walter Manucha<sup>1,2</sup>

<sup>1</sup>Instituto de Medicina y Biología Experimental de Cuyo (IMBECU), Consejo Nacional de Investigaciones Científicas y Técnicas (CONICET), Mendoza, Argentina

<sup>2</sup>Instituto de Fisiología, Facultad de Ciencias Médicas, Universidad Nacional de Cuyo, Mendoza, Argentina

<sup>3</sup>Instituto de Histología y Embriología “Dr. Mario H. Burgos” (IHEM), Consejo Nacional de Investigaciones Científicas y Técnicas (CONICET), Mendoza, Argentina

<sup>4</sup>Department of Pediatrics, Nephrology Division, Miller School of Medicine, University of Miami, Miami, FL, USA

## Correspondence

Emiliano Raúl Diez, Instituto de Fisiología, Facultad de Ciencias Médicas, Universidad Nacional de Cuyo, Mendoza, Argentina.  
Email: diez.emiliano@fcm.uncu.edu.ar

## Funding information

This work was supported by grants from Secretaría de Ciencia, Técnica y Postgrado, Universidad Nacional de Cuyo, awarded to A. Z. Ponce Zumino, E. R. Diez and W. Manucha, and PICT 2012-0234 from ANPCyT (Agencia Nacional de Promoción de la Ciencia y la Tecnología) awarded to W. Manucha.

## Abstract

Lethal ventricular arrhythmias increase in patients with chronic kidney disease that suffer an acute coronary event. Chronic kidney disease induces myocardial remodeling, oxidative stress, and arrhythmogenesis. A manifestation of the relationship between kidney and heart is the concomitant reduction in vitamin D receptor (VDR) and the increase in angiotensin II receptor type 1 (AT<sub>1</sub>). Melatonin has renal and cardiac protective actions. One potential mechanism is the increase in the heat shock protein 70 (Hsp70)—an antioxidant factor. We aim to determine the mechanisms involved in melatonin (Mel) prevention of kidney damage and arrhythmogenic heart remodeling. Unilateral ureteral-obstruction (UUO) and sham-operated rats were treated with either melatonin (4 mg/kg/day) or vehicle for 15 days. Hearts and kidneys from obstructed rats showed a reduction in VDR and Hsp70. Associated with AT<sub>1</sub> up-regulation in the kidneys and the heart of UUO rats also increased oxidative stress, fibrosis, apoptosis, mitochondrial edema, and dilated crests. Melatonin prevented these changes and ventricular fibrillation during reperfusion. The action potential lengthened and hyperpolarized in melatonin-treated rats throughout the experiment. We conclude that melatonin prevents renal damage and arrhythmogenic myocardial remodeling during unilateral ureteral obstruction due to a decrease in oxidative stress/fibrosis/apoptosis associated with AT<sub>1</sub> reduction and Hsp70-VDR increase.

## KEYWORDS

arrhythmias, chronic kidney disease, cytoprotective effects, melatonin, obstructive nephropathy, oxidative stress, reperfusion injury

## 1 | INTRODUCTION

Ventricular arrhythmias are prevalent and a major cause of mortality in patients with chronic kidney disease (CKD),<sup>1-3</sup> even when these patients are not suffering from electrolyte imbalances.<sup>4</sup> The mortality risk also increases in CKD patients

that suffer from an acute coronary syndrome.<sup>5</sup> Despite the increased numbers of cardiovascular events in patients with chronic kidney disease, there is a lack of specific treatments for these related diseases.

Regarding the pathogenic mechanisms that relate cardiac and renal diseases, our laboratory has recently

demonstrated that unilateral ureteral obstruction in rats is an adequate experimental model of chronic kidney disease that induces myocardial remodeling with increased arrhythmogenesis.<sup>6</sup> This remodeling includes a reduction in myocardial vitamin D receptor expression linked to increased angiotensin II receptor type 1 expression, fibrosis, mitochondrial edema, and a higher incidence of reperfusion arrhythmias; and all of them could be related to oxidative stress.

Melatonin is a well-known antioxidant that protects against kidney and heart injuries in different models. Melatonin and its metabolites have a direct free radical scavenger activity.<sup>7-9</sup> Endogenous circadian Melatonin secretion is impaired during chronic kidney disease.<sup>10</sup> While the exact cause and effect relationship is unclear, the impairment is related to the degree of chronic kidney disease and worsens with the progression of CKD.<sup>11</sup> Therefore, Melatonin plays a role in renal physiology, and in the pathogenic mechanisms of renal diseases, such as ureteral obstruction.<sup>12</sup> During unilateral ureteral-obstruction (UUO) development, melatonin treatment increases antioxidant capacity; decreases lipid peroxidation and the expression of iNOS, p65-NF- $\kappa$ B, and p38-MAPK; and reduces leukocyte infiltration, tubular injury, and interstitial fibrosis.<sup>13</sup> Additionally, melatonin increases the heat shock proteins as part of its protective effects.<sup>14</sup> In particular, melatonin induces heat shock protein 70—an anti-apoptotic protein—and protects the liver from toluene-induced oxidative stress.<sup>15</sup> Therefore, it could be postulated that the anti-apoptotic effects of melatonin might be responsible, at least in part, for the modulation of Hsp70.

Past studies show that melatonin has a role in protecting against oxidative damage caused by ischemia-reperfusion injury in the kidneys, testes, brain, and heart; both in vivo and in vitro.<sup>16-18</sup> Melatonin and vitamin D combination protect from renal ischemia-reperfusion injury.<sup>19</sup> The combined protective role involves the reduction of oxidative stress and enhanced nitric oxide (NO) bioavailability. A specific cardioprotective effect of melatonin in cardiorenal syndrome has been suggested.<sup>20</sup> Chua et al demonstrated that melatonin reverses structural and functional changes, mainly through the reduction of oxidative stress, mitochondrial and DNA damage, inflammation, and apoptosis. However, its anti-apoptotic and antiarrhythmic properties in UUO-induced nephropathy have not yet been investigated.

Finally, based on the above arguments, we decided to evaluate the following hypothesis: melatonin prevents kidney damage and heart remodeling in an animal model of CKD due to a reduction in oxidative stress/fibrosis/apoptosis mediated by an AT<sub>1</sub> and Hsp70-VDR modulation. To highlight, we also assessed whether this modulation is associated with structural changes or influences the electrophysiological response to ischemia-reperfusion injury.

## 2 | MATERIALS AND METHODS

### 2.1 | Ethics statement

All animals were cared for by the Guiding Principles in the Care and Use of Animals of the US National Institutes of Health. All procedures were authorized by the Institutional Animal Care and Use Committee of the School of Medical Sciences, Universidad Nacional de Cuyo (Approval ID: 48/2015).

### 2.2 | Surgical procedure and pharmacological treatment

The left ureters of male Wistar-Kyoto rats (weighing from 200 to 220 g) were surgically obstructed while under 60 mg/kg of ketamine and 0.1 mg/kg of acepromazine, as previously described. Briefly, for each test subject, the left ureter was completely ligated with silk at the union between the pelvis and proximal ureter, through a midline abdominal incision. Members of the control group underwent sham surgery. After the surgical closure of the abdominal incision, the rats received free access to water and food. After 15 days, the hearts and kidneys were harvested from both the obstructed and the sham-operated animals. The criterion for successful ureteral obstruction was the achieving of a ureteral dilation of greater than 2 mm (determined using a millimetric eyepiece).

Both groups (sham and obstructed) were treated either with water (vehicle) or with water supplemented with melatonin (Sigma-Aldrich, St. Louis, MO, USA) both offered *ad libitum* (stored in bottles protected from the light with aluminum foil). The treatment lasted 15 days (from surgery until euthanasia) and the dosage consisted of 3-5 mg/kg/day (average adjusted concentration by weight and water consumption). Thus, the following 4 groups were formed: sham + vehicle (Sham), sham + melatonin (Sham + Mel), obstructed (UUO), and obstructed + melatonin (UUO + Mel). Each of the 4 groups consisted of 5 animals to be used for the molecular and structural studies and 8 animals assigned to the ischemia-reperfusion experiment. Animals were euthanized with a lethal injection of pentobarbital. The serum urea and creatinine concentrations were determined using colorimetric assays (Sigma kits).

### 2.3 | Histological studies

Myocardial/renal tissue samples from 5 hearts/kidneys from each group were fixed in 10% phosphate-buffered formalin (pH = 7.1) for 24 to 48 hours before being embedded in paraffin and serially sectioned (5  $\mu$ m) on a microtome (Leica). The paraffin sections were subjected

to staining with Masson's trichrome stain, as previously described.<sup>6</sup>

## 2.4 | Identification of cellular apoptosis by TUNEL

After the digesting and quenching steps, an equilibration buffer was applied directly to the sections after which working strength TdT enzyme was directly applied. A biotin-conjugated anti-digoxigenin antibody (Sigma) was used. Then, the sections were incubated with biotinylated anti-mouse IgG (Dako, Carpinteria, CA, USA) at a 1:100 dilution for 45 minutes and later with peroxidase-labeled streptavidin (strept AB Complex/HRP; Dako) at a 1:100 dilution for 45 minutes. After a brief wash, 3,3'-diaminobenzidine tetrahydrochloride (0.5 mg/mL)/H<sub>2</sub>O<sub>2</sub> (0.01%), a chromogen substrate, was incorporated. For positive control, sections from involuting prostates were used (n = 2). For the quantification of apoptotic cells in cross-sectioned areas, 10 consecutive fields were randomly selected and were evaluated at 400×, on a 10 × 10 grid, using an image analyzer.

## 2.5 | Interstitial fibrosis assessment

For all morphologic evaluations were performed by an observer blinded to the origin of the histological sections. The myocardial/renal interstitial fibrosis was assessed in samples stained by Masson's trichrome method.<sup>21,22</sup> Blue-stained areas were determined as fibrosis and quantified by an image analyzer (Image-Pro Plus, Bethesda, MD, USA). Ten consecutive fields were randomly selected in the ventricular/cortex tissue and were evaluated at 400× on a 10 × 10 grid-imprinted reticule. The number of grid points containing blue collagen staining in the interstitium was divided by the total number of points in the fields to obtain the percentage of the fractional area of interstitial collagen deposition.

## 2.6 | Electron microscopy

Tissue samples from 5 hearts/kidneys were fixed by immersion in a fixative solution (1:10). The fixative solution was obtained by diluting 1 phosphate buffered saline (PBS) tablet, following the manufacturer's instructions, in 200 mL of double-distilled water and 2% glutaraldehyde (v/v), 2% of fresh p-formaldehyde (v/v), and 2% of picric acid as a saturated solution. After 2 hours at room temperature, the samples were reduced and placed in an OsO<sub>4</sub> solution overnight at 4°C. The next day, the samples were dehydrated in alcohol-acetone grading up to 100% and embedded in Epon 812 (Sigma). Ultrathin sections were obtained with an Ultracut microtome (Leitz) and stained with lead citrate and uranyl using conventional staining methods. Observations were made, and micrographs created using a Zeiss 900 microscope.

## 2.7 | Mitochondria isolation from myocardial and kidney tissues

All steps were carried out at 4°C. To ~200 mg of tissue were added 5 mL of mitochondrial isolation buffer (10 mmol/L HEPES pH 7.4, 70 mmol/L sucrose, 200 mmol/L mannitol, 1 mmol/L EDTA, protease inhibitor cocktail; Sigma, St. Louis, MO, USA). The tissue was homogenized with a Dounce glass homogenizer (Wheaton, catalog no. 357544). The lysate was then subjected to centrifugation at 1000 g for 10 minutes, yielding a nuclear pellet and postnuclear supernatant. The heavy mitochondrial fraction was obtained from the postnuclear supernatant after centrifugation at 3000 g for 10 mol/L. This pellet was resuspended, and the 3000 g spin was repeated to obtain the final heavy mitochondrial pellet. The supernatant resulting from the 3000 g spins was then subjected to 15 000 g for 10 minutes. The resulting light mitochondrial pellet was resuspended, and sequential 3000 and 15 000 g spins yielded the final light mitochondrial pellet. The purity of the mitochondrial fractions was established as previously described<sup>23</sup> with minor modifications.

## 2.8 | NADPH oxidase activity assay from isolated mitochondria

Cytotoxicity from oxidative stress arises when excess reactive oxygen species (ROS) accumulate in the host's defense mechanisms. In this context, NADPH oxidase activity is one of the elements highly involved in apoptosis induction. NADPH oxidase activity was measured using Luminol (5-amino-2, 3-dihydro-1,4-phthalazine; SIGMA). Samples were homogenized and centrifuged at 6000 rpm for 30 min. The supernatant was separated and again centrifuged (at 19 500 rpm), and the protein concentration of the membrane fraction lysate was quantified by Lowry assay using bovine serum albumin as a standard. A sample (40 µL) of the membrane fraction resuspended in lysis buffer was rapidly read in the spectrofluorometer (Fluoro Count TM; AF10001, Cambers Company, USA) to establish the basal value of each sample. Then, 2 µL of β-NADH (Sigma), 0.1 mmol/L and 2 µL of Luminol 5 µmol/L in dimethyl sulfoxide were incorporated and read for 10 minutes (360 nm excitation and 460 nm emission). The values were indicated as relative fluorescence units per micrograms of protein and per min of incubation.

## 2.9 | Reverse transcription polymerase chain reaction and semi-quantification of mRNA for VDR, AT<sub>1</sub>, Hsp70, and β-Actin

Total ribonucleic acid from ventricular myocardial and kidney cortex tissue was obtained using Trizol reagent (Gibco

**TABLE 1** Sets of primers for RT-PCR

Primer	Sequence	Annealing C°	Predicted product size, bp
VDR			
Sense	5'-GACTTTGACCGGAACGTGCG-3'	62	227
Antisense	5'-CATCATGCCGATGTCCACAC-3'		
AT <sub>1</sub>			
Sense	5'-GCACACTGGCAATGTAATGC-3'	55	385
Antisense	5'-GTTGAACAGAACAAAGTGACC-3'		
Hsp70			
Sense	5'-CCGCCTACTTCAACGACTC-3'	56	291
Antisense	5'-TCTTGAACTCCTCCACGAAG-3'		
β-Actin			
Sense	5'-TGGAGAAGAGCTATGAGCTGCCTG-3'	65	201
Antisense	5'-GTGCCACCAGACAGCACTGTGTTG-3'		

BRL). One microgram of ribonucleic acid was denatured in the presence of 0.5 µg/50 µL of oligo(dT) 15 primer and 40 U of recombinant ribonuclease inhibitor (Promega, USA). Reverse transcription was performed in the presence of the mixture using 200 units of reverse transcriptase in reaction buffer and 0.5 mmol/L of deoxyribonucleotides triphosphate, each, and incubated for 60 minutes at 42°C. The complementary DNA (10 µL) was amplified by polymerase chain reaction under standard conditions. Each sample was measured for VDR, AT<sub>1</sub>, Hsp70, and β-actin (primers in Table 1, Integrated DNA Technologies, Inc.). The VDR, AT<sub>1</sub>, and Hsp70 signals were standardized against the β-actin signal for each sample, and the results were expressed as a ratio.

## 2.10 | Immunohistochemical studies

The kidney and heart paraffin sections were processed according to a previously described technique.<sup>24</sup> The antibodies applied were rabbit polyclonal antibody against AT<sub>1</sub> (306), rabbit polyclonal antibody against Hsp70 (H-300), and mouse monoclonal antibody against VDR (D-6) (Santa Cruz Biotechnology, Inc.), each of which was diluted at 1:500. A commercial immunoperoxidase kit was used (Dako). The positive reaction was evaluated regarding the specific location of the immunostaining and the intensity of the immunoreaction. The negative controls included tissues unexposed to primary antibodies as well as tissues exposed to control immunoglobulin G. The positive controls were human breast cancer biopsy samples. The immunostaining was evaluated and resolved by consensus according to a scoring system reported previously.<sup>25,26</sup> Briefly, we used the following intensity scores: 0 = no staining; 1 = weak staining; 2 = moderate staining; and 3 = strong staining.

## 2.11 | Immunofluorescence confocal microscopy

The kidneys and hearts were washed twice with PBS, placed in isopentane, and stored at -70°C. Tissue sections (10 µm) were obtained using a cryostat. Each section was gelatinized and fixed by paraformaldehyde buffer overnight at 4°C. After the fixation procedure, the sections were cryoprotected in a PBS solution supplemented with 0.9 mol/L of sucrose overnight at 4°C. After neutralization with NH<sub>4</sub>Cl buffer, the sections were permeabilized for 45 min with 0.05% saponin/PBS (pH = 7.4) and incubated overnight with the following primary antibodies: polyclonal anti-AT<sub>1</sub> (1:100) (Santa Cruz Biotechnology) and monoclonal anti-Hsp70 (1:100) (Sigma Aldrich). Secondary antibodies were donkey anti-mouse IgG antibody, Cy3 conjugated (1:750) and goat anti-rabbit IgG antibody, Cy2 conjugated (1:750). The tissues were stained with Hoechst 33342 (10 nmol/L) for 5 min. The coverslips were mounted in Fluoroshield solution (Sigma Aldrich) for confocal microscopy. Confocal immunofluorescence images were taken using the FV10-ASW 1.7 software and the Olympus IX81 microscope. Images were processed and analyzed using ImageJ. The immunofluorescence was evaluated and resolved by consensus according to a scoring system reported previously.<sup>27,28</sup> Briefly, we used the following intensity scores: 0 = no staining; 1 = weak staining; 2 = moderate staining; and 3 = strong staining.

## 2.12 | Langendorff-perfused rat hearts

After euthanasia, 8 hearts from each group were rapidly excised and connected to a perfusion system. The hearts were perfused at a constant pressure of 80 cm H<sub>2</sub>O with a

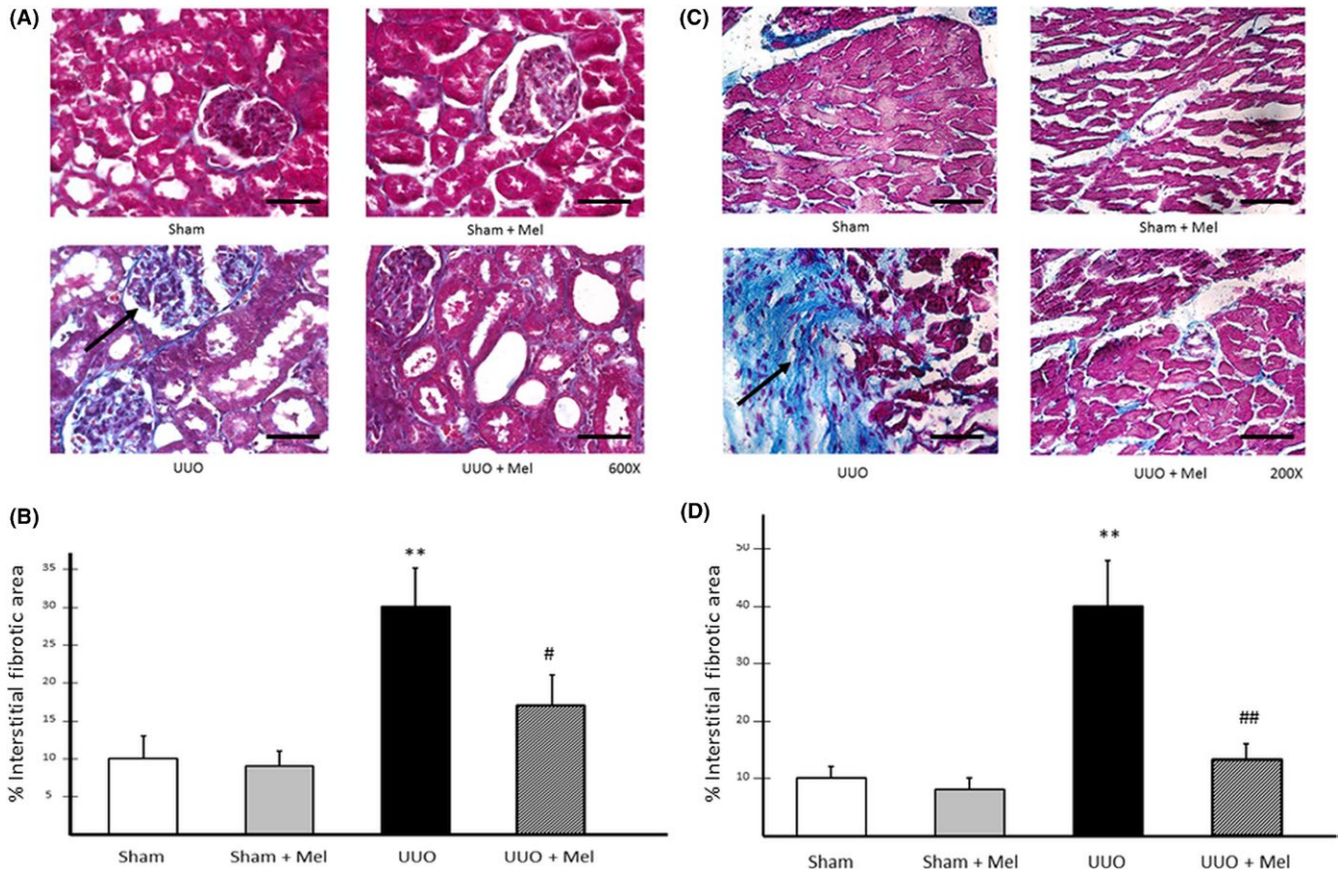


**FIGURE 1** Masson's trichrome in renal cortices and myocardial tissue: Melatonin's effect on collagen deposition during UUO. A, Representative kidney cortex pictures from vehicle-treated rats (Sham), Mel-treated rats (Sham + Mel), obstructed and vehicle-treated rats (UUO), and obstructed and Mel-treated rats (UUO + Mel). Collagen deposition is stained blue (arrowheads), nuclei are stained dark red/purple, and cytoplasm is stained red/pink. The scale bars (black) indicate 50  $\mu$ m. B, Masson's trichrome quantification from renal tissue. The interstitial fibrotic area of the UUO revealed a significant expansion of the interstitial space compared to what was seen in the Sham rats. Conversely, in UUO + Mel group the expansion of the interstitial space was significantly decreased in comparison to that of the UUO rats. The cortices of the Sham + Mel group did not show differences in relation to those of the Sham group. C, Representative myocardial tissue. D, Masson's trichrome quantification. The interstitial fibrotic area of the myocardia from UUO rats revealed a significant expansion of the interstitial space compared with the myocardia from the subjects in the Sham group. Melatonin after unilateral obstruction (UUO + Mel) decreased myocardial fibrosis and remodeling in comparison to UUO. Results are means  $\pm$  SEM of 5 independent observations. \*\* $P < .01$  vs both Sham and Sham + Mel, # $P < .05$  and ## $P < .01$  vs UUO

modified Krebs-Henseleit solution containing the following (in mmol/L): 121 NaCl, 25 NaHCO<sub>3</sub>, 1.2 Na<sub>2</sub>HPO<sub>4</sub>, 5 KCl, 2.5 CaCl<sub>2</sub>, 1.2 MgSO<sub>4</sub>, and 11 glucose. When equilibrated with 5% CO<sub>2</sub> in O<sub>2</sub> at 36.5 ( $\pm$ 0.5) °C, the pH was 7.40 ( $\pm$ 0.02).

Coronary flow was measured throughout the experiment and was used as an index of adequate perfusion and as a criterion to assess the efficacy of the coronary ligation. A reduction of at least 25% during occlusion was considered

satisfactory to guarantee the reproducibility of reperfusion arrhythmia incidence.<sup>27</sup>

### 2.13 | Reperfusion arrhythmias and action potentials

After 20 minutes of stabilization, we continuously obtained the surface electrogram equivalent of lead II and epicardial transmembrane potential using a Hewlett-Packard 1500A

**TABLE 2** Biochemical parameters in UUO: Melatonin effect

	Sham	Sham + Mel	UUO	UUO + Mel
Creatinine (mg/dl)	0.60 $\pm$ 0.05	0.58 $\pm$ 0.04	0.70 $\pm$ 0.05	0.65 $\pm$ 0.03
Urea (mg/dl)	41 $\pm$ 4	39 $\pm$ 5	47 $\pm$ 4	42 $\pm$ 3

Results are means  $\pm$  SEM of 13 independent observations.

and a custom made microelectrode amplifier, respectively. Both signals were digitized with an analog-to-digital converter (NI PCI-6221; National Instruments, USA) and recorded using LabView SignalExpress 2.5. After 10 minutes of pre-ischemia, the left anterior descending coronary was ligated during 10 minutes and followed by 10 minutes of reperfusion. Ventricular arrhythmias were classified according to the Lambeth convention.<sup>28</sup> We evaluated the incidence and duration of ventricular tachycardia (VT) and ventricular fibrillation (VF). We also evaluated the severity of the arrhythmias each minute using the following scores: 0 = sinus rhythm; 1 = premature ventricular beats or bigeminy; 2 = salvos; 3 = nonsustained VT (<30 seconds); 4 = sustained VT (>30 seconds) or VF.<sup>29</sup> We analyzed the following parameters of epicardial

transmembrane potentials: action potential amplitude, resting potential, and action potential duration at 50% and 90% of repolarization.

## 2.14 | Statistical analysis

Data were expressed as mean  $\pm$  SEM, and statistical analysis was performed using ANOVA or two-way repeated measures ANOVA followed by a Bonferroni posttest. Incidence of arrhythmias was compared by Fisher's exact test. Variables not normally distributed were analyzed using the Kruskal-Wallis test followed by Dunn's posttest. A *P*-value of <.05 was considered to be significant. Statistical analysis was performed using GraphPad Prism 5.0 (GraphPad Software, Inc., La Jolla, CA, USA).

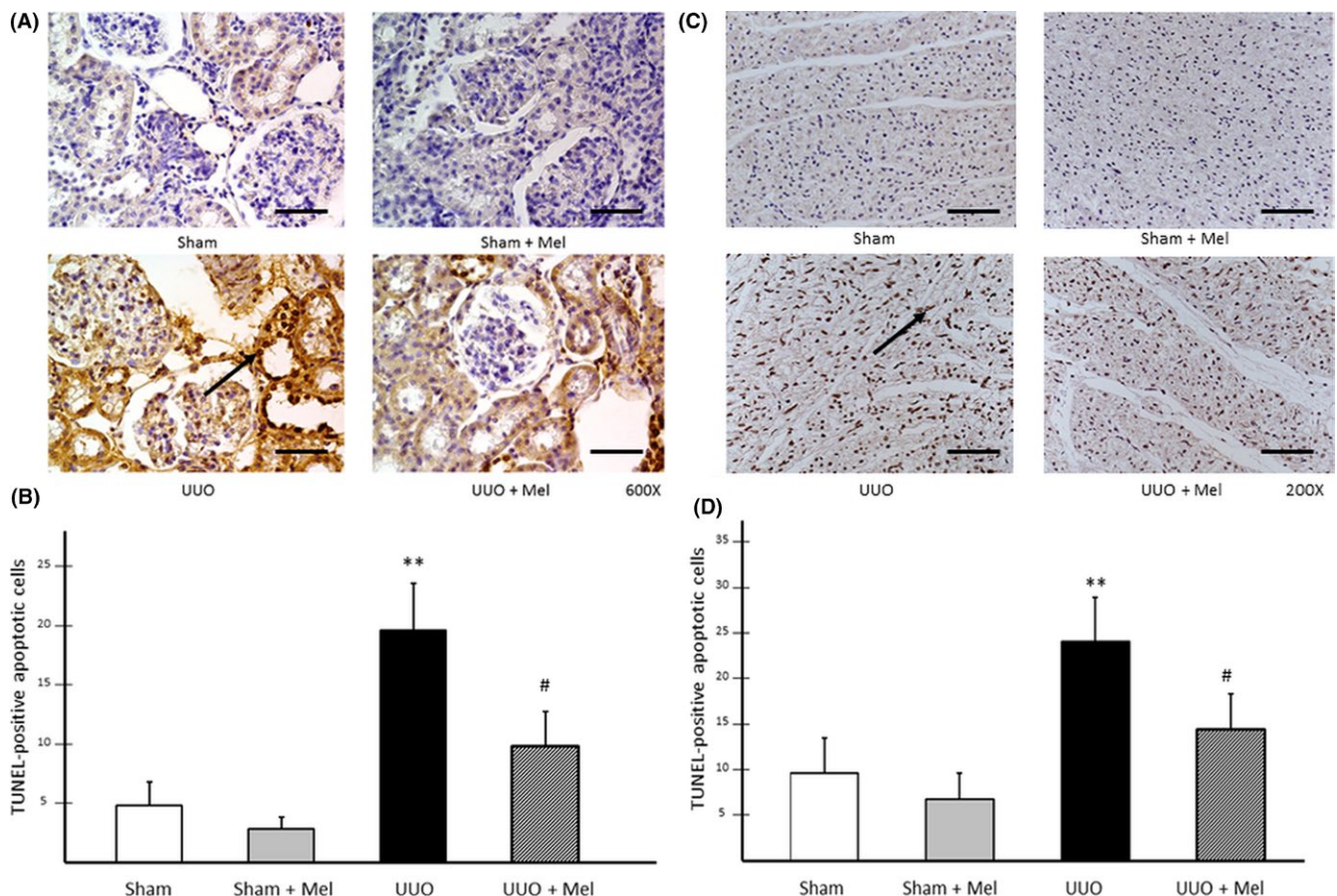


**FIGURE 2** Identification and quantification of cellular apoptosis using the TUNEL technique in renal cortices and myocardium: Melatonin's effect on cell death during UUO. A, Localization of apoptotic nuclei by TdT-uridine-nick-end-labeling technique (TUNEL). Representative kidney cortex pictures from Sham, Sham + Mel, UUO, and UUO + Mel groups. Positive apoptotic nuclei appear as heavy brown-stained nuclei (arrowheads) in glomerular, tubule epithelial cells. The scale bars indicate 50  $\mu$ m. B, Quantification of apoptotic cells in cortices. The number of TUNEL-positive nuclei increased in glomerular and tubular epithelial cells from UUO compared with the Sham-treated animals. In UUO+Mel group, the apoptotic nuclei decreased in comparison to UUO. C, Representative TUNEL staining of myocardial tissue from the 4 groups as indicated below the pictures. The UUO increased apoptosis in cardiomyocytes (arrows indicate apoptotic nucleus) and melatonin prevented from this type of cell death. The scale bars indicate 100  $\mu$ m. D, Quantification of apoptotic cells in the myocardium. The heart from UUO rats increased the number of TUNEL-positive nuclei compared to the Sham-treated animals. Melatonin reduced the apoptosis induced by unilateral obstruction. Results are means  $\pm$  SEM of 5 independent observations. \*\**P* < .01 vs both Sham and Sham + Mel; and #*P* < .05 vs UUO

### 3 | RESULTS

#### 3.1 | Serum chemistries

In the UUO group, the analytical data of the blood biochemistry showed a slight increase in the measured parameters (urea and creatinine) that was without statistical significance. These slight trends were absent in those animals that received Mel (Table 2).

#### 3.2 | Melatonin's effects on interstitial fibrosis, apoptosis, NADPH oxidase activity, and mitochondrial ultrastructural changes during UUO

The renal cortices of the UUO kidneys showed higher (threefold) collagen accumulation in the expanded interstitium in relation to the renal cortices of the Sham group

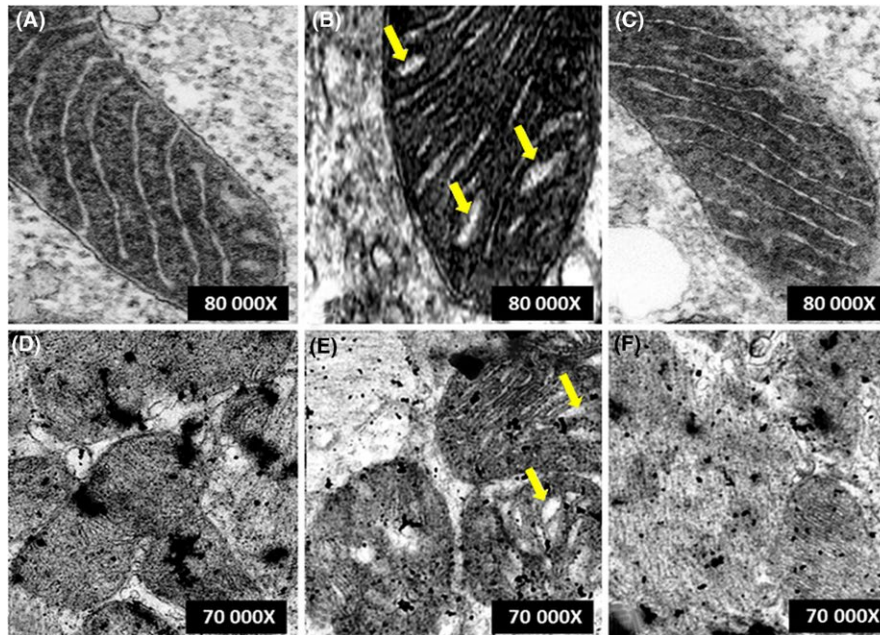


**FIGURE 3** Electron microscopy and NADPH oxidase activity studies in the renal cortices and heart during UUO: Melatonin's effect. Upper panel: A, Electron microscopy of the cortical cortices of Sham-treated animals. B, Electron microscopy of the cortical cortices of UUO-treated animals. C, The same experimental conditions as in B, but with melatonin treatment (UUO + Mel). D, Electron microscopy of the myocardia of Sham-treated animals. E, Electron microscopy of the myocardia of UUO-treated rats. F, The same experimental conditions as in E, but with melatonin treatment (UUO + Mel). Mitochondria are present in the spaces between the dilated mitochondrial cristae (arrows in B and E) in untreated kidneys and myocardia. Lower panel: Representative graphics of NADPH oxidase activity quantification in mitochondrial fractions from kidneys and hearts are shown. NADPH oxidase activity from kidneys and hearts was significantly greater in UUO animals than it was in those of the Sham group. However, NADPH oxidase activity from kidneys and hearts was more reduced in UUO + Mel animals than it was in those of the UUO group. No differences were observed in the kidney cortices and myocardia from Sham + Mel animals about what was observed in the Sham group. Results are means  $\pm$  SEM of 5 independent observations. \* $P < .05$  and \*\* $P < .01$  vs both Sham and Sham + Mel; and # $P < .05$  vs UUO

(see Figure 1A,B). In comparison to those of the UUO group, kidneys treated with Mel showed lower collagen accumulation in the expanded interstitium, along with cellular interstitial infiltrates in the cortex. The kidneys of the Sham and Sham + Mel had no differences in the interstitial collagen deposition.

The microscopic structure of the hearts revealed evidence of increased fibrosis. The hearts from Sham + Mel did not appear to be any different from those of the Sham (Figure 1C,D). However, the hearts from UUO + Mel group showed lower collagen accumulation in the expanded interstitium, along with cellular interstitial infiltrates in relation to the UUO group.

The kidney cortices displayed in Figure 2A,B show an increased number of TUNEL-positive apoptotic cells in the glomerular and tubular epithelial cells from the UUO compared to those of the Sham group. The number of TUNEL-positive apoptotic cells in the UUO + Mel group was lower than was the number found in the untreated UUO group.

A TUNEL analysis of the hearts from the UUO group showed an increased number of apoptotic cells in comparison with those of the Sham group. Treatment with melatonin reduced apoptosis in myocardial cells from UUO (UUO + Mel) with respect to the UUO group. The distribution of apoptotic cardiomyocytes area was rather diffuse (Figure 2C,D). The kidneys and hearts of the Sham + Mel had no differences in the number of TUNEL-positive apoptotic cells compared to the Sham group.

Kidneys and hearts from the UUO group showed mitochondrial edema with dilated cristae (arrowheads in Figure 3B,E). Consistent with these ultrastructural findings, we demonstrate—in mitochondrial fractions—that NADPH oxidase activity was significantly higher in the UUO group than it was in the Sham group (lower panel of Figure 3). Melatonin prevented mitochondrial edema (Figure 3C,F), and lower NADPH oxidase activity (from kidneys and hearts). The Sham and Sham + Mel group show abundant mitochondria, mostly with normal ultrastructure and without significant differences in NADPH oxidase activity.

### 3.3 | Melatonin's effects on VDR, AT<sub>1</sub>, and Hsp70 renal/myocardial expression during UUO

Figure 4 shows VDR, AT<sub>1</sub>, and Hsp70 mRNA expression in the renal cortices (Figure 4A,B) and myocardia (Figure 4C,D) of all the groups. More specifically, VDR and Hsp70 mRNA analysis of the renal cortices from the UUO group showed significantly lower expression in comparison with those of the Sham group. The renal AT<sub>1</sub> mRNA expression revealed a twofold increase in the UUO group compared to the Sham group. Mel increased VDR and Hsp70 mRNA expression

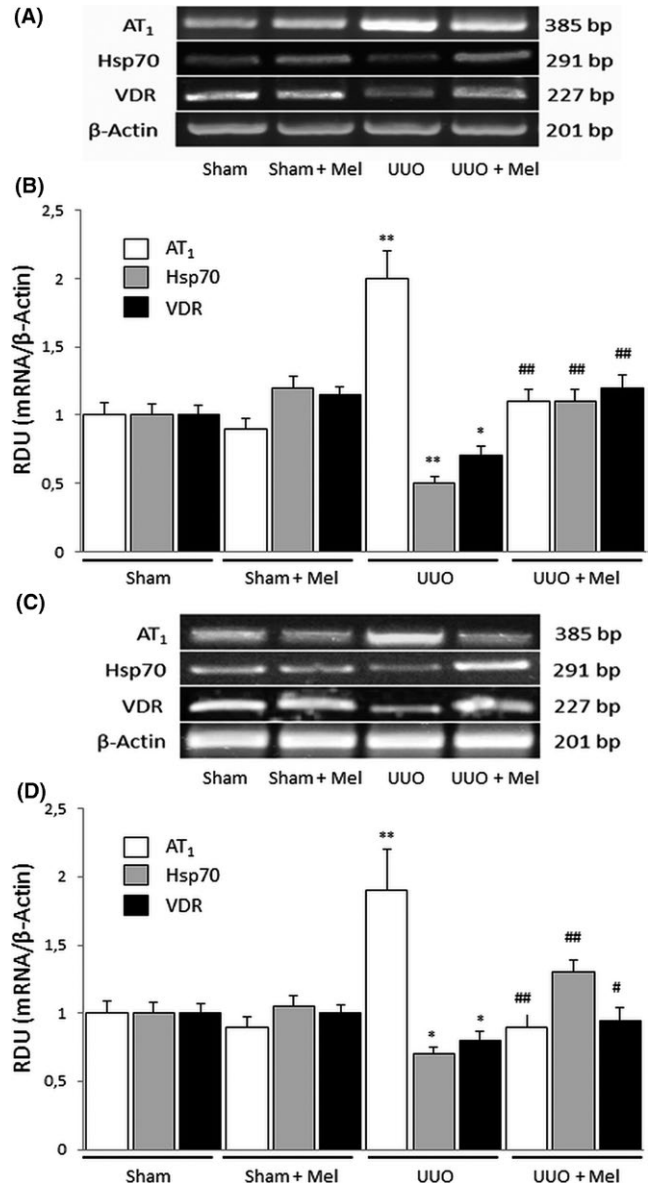


**FIGURE 4** mRNA expression by RT-PCR and semi-quantification of AT<sub>1</sub>, Hsp70, and VDR in UUO: Melatonin's effect. Representative gels of AT<sub>1</sub>, Hsp70, and VDR mRNA in the kidney cortices (A) and myocardia (C) of obstructed and Sham-operated rats treated or not with Mel, are shown. The corresponding housekeeping  $\beta$ -actin is included below (A and C). The relative amount of mRNA expression was determined after normalization of the level of AT<sub>1</sub>, Hsp70, and VDR mRNA of the appropriate control and is shown in histograms beneath the corresponding blots (B and C). Renal cortices and myocardial tissue from UUO animals showed higher expression of AT<sub>1</sub> and lower expression of VDR and Hsp70 mRNA in comparison with those of the Sham animals. In UUO + Mel animals, melatonin decreased of AT<sub>1</sub> mRNA and restored VDR expression in renal cortices and ventricles. Melatonin preserved Hsp70 mRNA expression in the kidneys and increased its expression in the hearts of UUO animals. Results are means  $\pm$  SEM of 5 independent observations. \* $P$  < .05 and \*\* $P$  < .01 vs Sham; # $P$  < .05 and ## $P$  < .01 vs UUO

and decrease in AT<sub>1</sub> mRNA expression in the renal cortices of the UUO (UUO + Mel) group compared to those of the untreated UUO group (Figure 4A,B). As was observed in the renal cortices, the myocardial mRNA expression of VDR and Hsp70 decreased and AT<sub>1</sub> increased in the UUO group. Mel restored of VDR and Hsp70 mRNA expression in the myocardia and decreases in AT<sub>1</sub> mRNA expression (Figure 4C,D).

In support of the transcriptional results (mRNAs), Figures 5 and 6 shown VDR, AT<sub>1</sub>, and Hsp70, while Figures 7 and 8 show AT<sub>1</sub> and Hsp70 protein expression in the renal cortices and myocardia from all groups. Immunocytochemical (Figures 5 and 6) and immunofluorescence (Figures 7 and 8) analyses were performed to establish protein location and immunoreaction intensity.

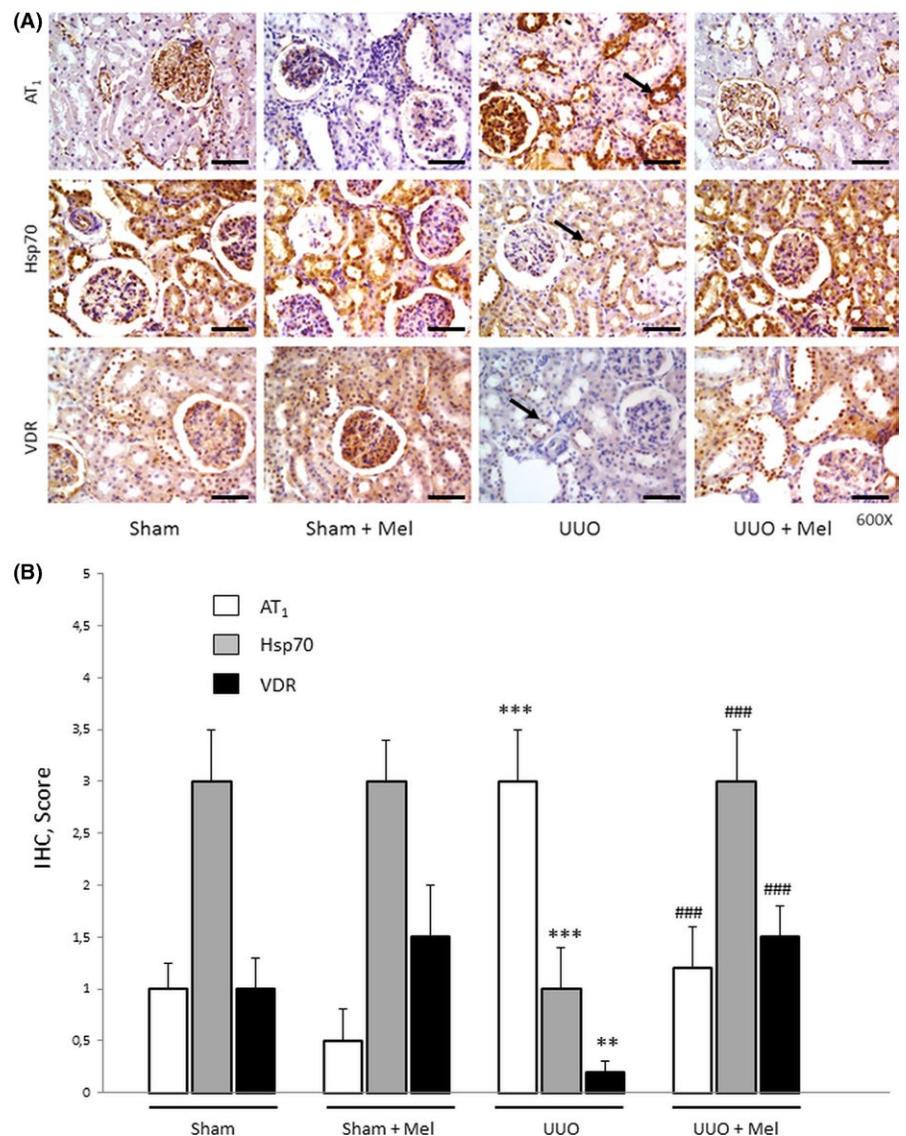
The renal cortices and myocardial tissue of the UUO group showed low levels of vitamin D receptor and Hsp70 immunostaining, as well as a low level of Hsp70 immunofluorescence (Figures 5-8). A very high level of AT<sub>1</sub> staining

was shown in the renal cortices and myocardia of the UUO compared to Sham groups. For details see arrowheads for AT<sub>1</sub> in Figures 5A, 6A, 7A,B, and 8A. Mel treatment induced a higher VDR and Hsp70 and a reduction in AT<sub>1</sub> immunostaining/fluorescence compared to those of the untreated UUO group.

### 3.4 | Electrophysiological effects of melatonin

During ischemia, premature ventricular complexes developed in half of the hearts of the members of the UUO group. Most arrhythmias started a few seconds after reperfusion (Figure 9A). Salvos were seen in all the groups. Ventricular tachycardia was frequent in the Sham and UUO groups (Figure 9A,B). Ventricular fibrillation increased only in the UUO group. A sample of this lethal arrhythmia is evident in Figure 9. Melatonin effectively prevented severe reperfusion arrhythmias. The arrhythmic episodes were shorter

**FIGURE 5** Immunohistochemistry (IHC) technique and semi-quantification of AT<sub>1</sub>, Hsp70, and VDR expression in kidney cortices from UUO-treated animals: Melatonin's effect. A, Representative pictures of kidney cortices from vehicle-treated rats (Sham), Mel-treated rats (Sham + Mel), obstructed and vehicle-treated rats (UUO), and obstructed and Mel-treated rats (UUO + Mel). Positive AT<sub>1</sub>, Hsp70, and VDR protein expression appear as brown-stained nuclei and cytosol (arrowheads) in glomerular and tubular epithelial cells. The scale bars indicate 50  $\mu$ m. B, Quantitative assessments of IHC staining in kidney cortices. The IHC score from UUO animals revealed a very significant increase in AT<sub>1</sub> staining and a decrease for Hsp70 and VDR compared to that of the Sham animals staining. Melatonin prevented the changes in AT<sub>1</sub>, Hsp70 and VDR staining induced by UUO but not in respect to the Sham group. Results are means  $\pm$  SEM of 5 independent observations. \*\* $P$  < .01 and \*\*\* $P$  < .001 vs Sham; ### $P$  < .001 vs UUO



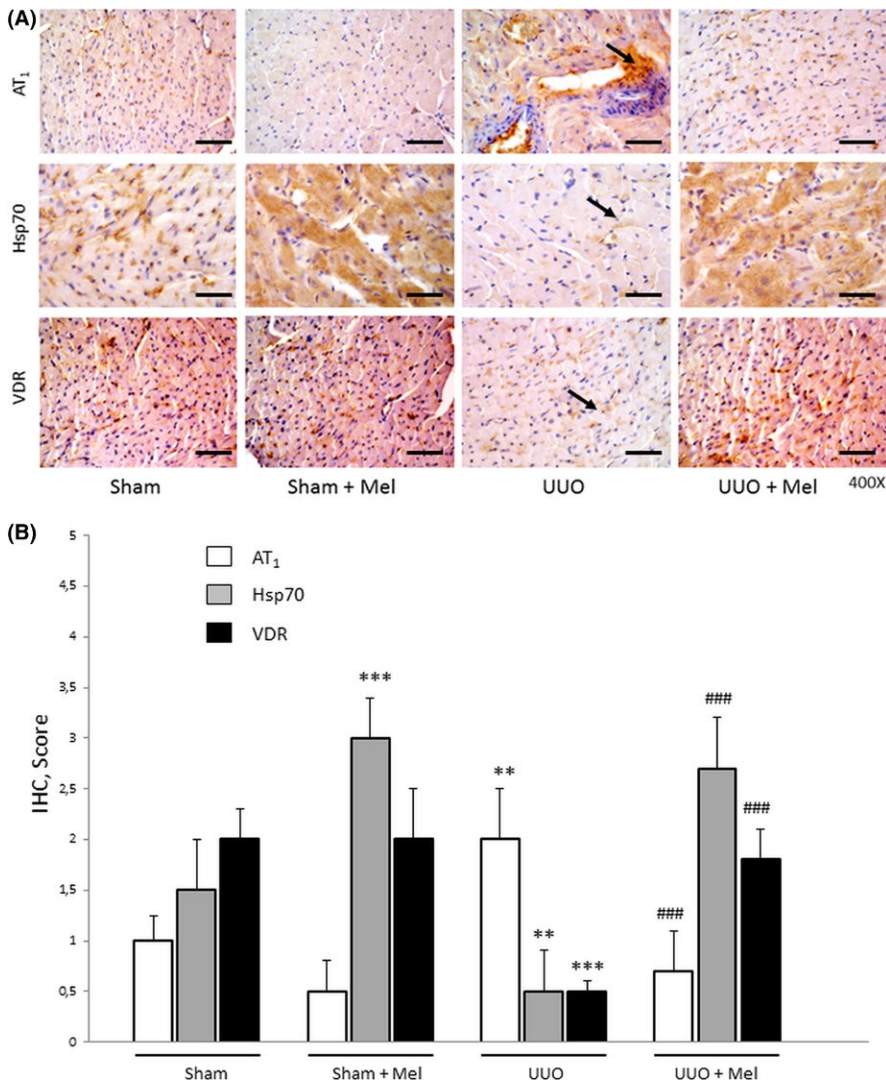


**FIGURE 6** Immunohistochemistry (IHC) technique and semi-quantification of AT<sub>1</sub>, Hsp70, and VDR expression in myocardium from UUO: Melatonin's effect. A, Representative IHC images from the myocardial tissue of the 4 groups, as indicated below each column of pictures. Positive AT<sub>1</sub>, Hsp70, and VDR protein expression appear as brown-stained nuclei and cytosol (arrowheads) in myocardial cells. The scale bars indicate 50 μm. B, Quantitative assessments of IHC staining in the myocardium. Melatonin increased the IHC score for Hsp70 in both treated group (Sham and UUO). In hearts from UUO, AT<sub>1</sub> staining increased but Hsp70 and VDR staining decrease compared to the Sham animals. In UUO + Mel group, AT<sub>1</sub> staining was significantly decreased in comparison to that of UUO alone ( $P < .001$ ). Results are means  $\pm$  SEM of 5 independent observations. \*\* $P < .01$  and \*\*\* $P < .001$  vs Sham; ### $P < .001$  vs UUO

with melatonin. The median duration of ventricular tachycardia decreased from 43 s (IQR 33–81 s) in the Sham group to 0 s (IQR 0–0 s) in the Sham + Mel group ( $P < .01$ ), and from 79 s (IQR 61–90 s) in the UUO group to 0 s (IQR 0–9 s) in the UUO + Mel group ( $P < .01$ ). In the hearts of the UUO group, the median duration of ventricular fibrillation increased to 290 s (IQR 157–415 s), while the other medians remained at 0 s (IQR 0–0 s) ( $P < .001$  vs. each group). The longer duration of ventricular tachycardia and fibrillation appeared to explain the higher arrhythmic scores in the members of the UUO group (Figure 9C).

Chronic melatonin treatment changed the epicardial action potential characteristics. Melatonin increased the amplitude in both treated groups throughout all the experimental periods (Figure 10). Concomitantly, melatonin hyperpolarized the resting potential. Hyperpolarization persisted during ischemia and reperfusion in treated hearts. Ischemia induced slight and progressive bradycardia, but the heart rate was the same for the members of the 4 groups. The treatment lengthened the action potential duration (measured at 50% and 90%

of the repolarization, from the stabilization period). During the first half of ischemia, all the hearts increased to the action potential duration. Before reperfusion, the action potential durations decreased in the hearts from the members of the UUO group to values shorter than stabilization values. During reperfusion, a progressive lengthening occurred in all groups.

## 4 | DISCUSSION

In this study, we demonstrate preventive actions of melatonin against kidney and heart damage induced by UUO. The protective mechanisms involve AT<sub>1</sub> reduction and Hsp70-VDR increase. New electrophysiological properties of chronic melatonin deserve notice, due to its relevance for cardiorenal situations with high arrhythmic risk and the lack of treatments.

The anti-inflammatory, anti-apoptotic, anti-fibrotic, and antioxidant properties of melatonin confer protection against several types of kidney disease.<sup>30,31</sup> Ozbek et al demonstrated

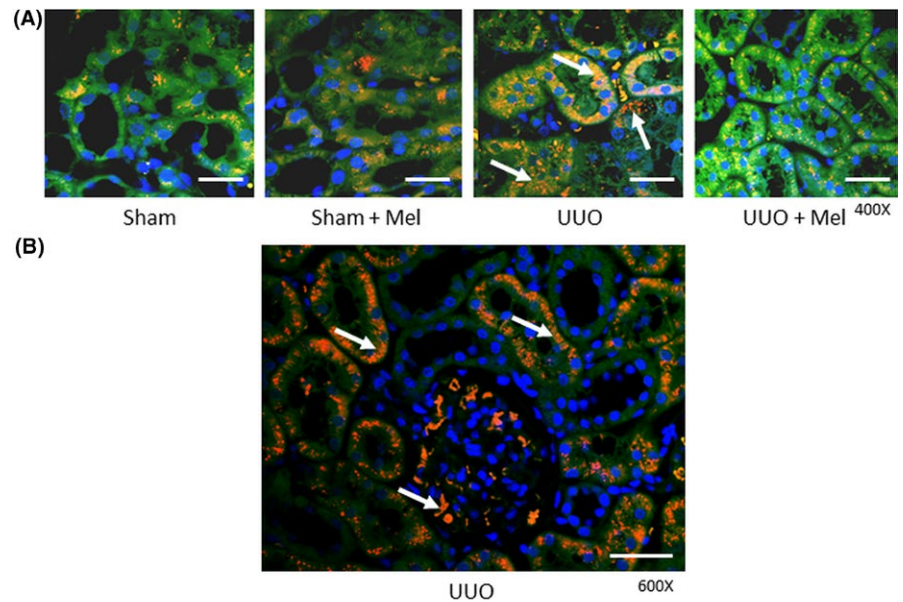
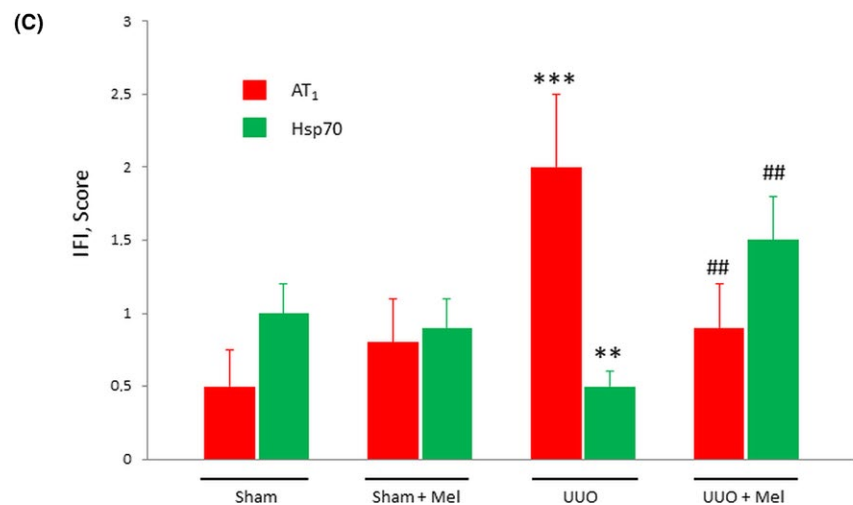


**FIGURE 7** Immunofluorescence (IFI) technique and semi-quantification of AT<sub>1</sub> and Hsp70 expression in kidney cortices from UUO: Melatonin's effect. A, Representative confocal microscopy IFI images of renal cortices from Sham, Sham + Mel, UUO, and UUO + Mel. B, Enlarged image of renal cortices from UUO rats. Positive IFI localization for AT<sub>1</sub> (arrowheads) appear on renal cortex tissues labeled in red and Hsp70 in green. Nuclei are in blue. The scale bars indicate 50  $\mu$ m. C, Quantitative assessments of immunofluorescence staining in renal cortices. Renal cortices IFI scores from UUO animals showed very high expression of AT<sub>1</sub> compared to those of the Sham animals (see arrows in A and B). Contrarily, Hsp70 expression was lower in UUO group. Melatonin treatment after UUO induced high Hsp70 immunofluorescence and reduced AT<sub>1</sub> intensity compared to UUO group. Results are means  $\pm$  SEM of 5 independent observations. \*\* $P < .01$  and \*\*\* $P < .001$  vs Sham; ## $P < .01$  vs UUO

that melatonin attenuates UUO-induced renal injury by reducing oxidative stress, tubular damage, and interstitial fibrosis and by increasing antioxidant capacity.<sup>13</sup> Recently, Yildirim et al reported that melatonin reduces apoptosis in kidneys submitted to UUO. However, the precise nature of melatonin-mediated cytoprotection and the mechanism by which it preserves the cardiorenal system from harm during UUO remain incompletely known. In relation to urea and creatinine measured in the serum of the rats, we don't observe differences between groups in any of the assessed parameters, suggesting that in the UUO model, 1 intact kidney is sufficient for sustaining renal function. The present study confirmed melatonin's anti-fibrotic, anti-apoptotic, and antioxidant effects (Figures 1-3, respectively) and linked them to an AT<sub>1</sub> reduction and Hsp70-VDR increase (Figures 4-8), which prevented kidney damage and arrhythmogenic heart remodeling (Figure 9).

In renal and myocardial tissue, melatonin increased Hsp70 and VDR and decreased AT<sub>1</sub> and fibrosis (see Figures 4-8).

Melatonin increases the HSPs as part of its antioxidant protective effect in tomatoes.<sup>14</sup> The activation of melatonin receptors MT1/MT2 increase the HSP in pancreatic cancer cells.<sup>32</sup> Of interest for our finding, melatonin increases Hsp70 and protects the livers of toluene-exposed rats from oxidative stress-induced cytotoxicity.<sup>15</sup> Hsp70 regulates antioxidant responses to cellular oxidative stress, and our laboratory showed that Hsp70 reduces the activity and expression of NADPH oxidase.<sup>33,34</sup> In agreement with our previous findings, we now demonstrate an increase in Hsp70 in melatonin-treated rats. Hsp70 induces VDR, facilitates the intracellular localization of active vitamin D metabolites, and transactivates vitamin D receptors.<sup>35</sup> Nuclear receptors of melatonin, as members of the retinoid-related orphan receptors, may interact and prevent vitamin D receptor degradation.<sup>36,37</sup> Myocardial VDR expression links CKD to cardiovascular disease because vitamin D receptor reduction amplifies the effects of angiotensin.<sup>38</sup> Unprecedentedly, melatonin decreased renal and myocardial AT<sub>1</sub> overexpression. It is well documented that



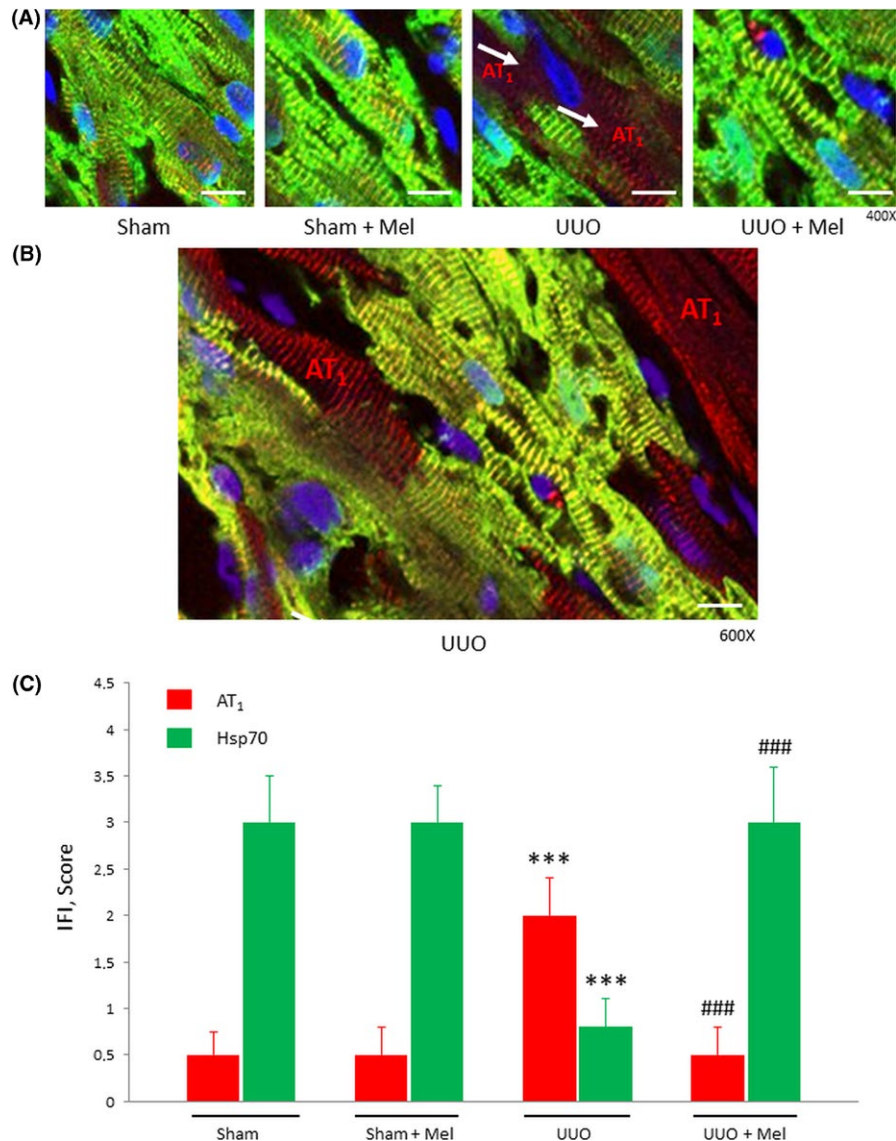


**FIGURE 8** Immunofluorescence (IFI) technique and semi-quantification of AT<sub>1</sub> and Hsp70 expression in myocardia from UUO: Melatonin's effect. A, Representative confocal microscopy IFI images of myocardia from the 4 group as indicated below each picture. B, Enlarged image of myocardial tissue from UUO rats. Positive IFI localization for AT<sub>1</sub> (arrowheads) appears on myocardial tissues labeled in red and Hsp70 in green. Nuclei were stained in blue. The scale bars indicate 50  $\mu$ m. C, Quantitative assessments of immunofluorescence staining in myocardium using the IFI score. Hearts of UUO group showed high AT<sub>1</sub> expression and low Hsp70 expression when compared to those of the Sham group. Melatonin treatment prevented the changes in both AT<sub>1</sub> and Hsp70 induced by UUO. Results are means  $\pm$  SEM of 5 independent observations. \*\*\* $P$  < .001 vs Sham; ### $P$  < .001 vs UUO

the AT<sub>1</sub> pathway leads to myocardial fibrosis during chronic kidney disease.<sup>6</sup> As previously suggested, low AT<sub>1</sub> expression through vitamin D receptor induction could be a consequence of Hsp70-mediated cell protection.<sup>39</sup> Interestingly, endogenous circadian melatonin secretion is impaired during chronic kidney disease.<sup>10</sup> In addition, angiotensin II exerts a tonic modulation of melatonin synthesis by influencing the activity of tryptophan hydroxylase via the AT<sub>1</sub>-receptors.<sup>40</sup> Our findings suggest that melatonin modulates AT<sub>1</sub> expression and that Hsp70 and VDR are key factors. The latter fact allows us to support the postulated feedback (or reciprocal regulation) between AT<sub>1</sub> and melatonin.

In close connection, mitochondrial dynamics is a point of interaction for circadian alterations in cardiovascular diseases linked the up-regulation of the renin-angiotensin-aldosterone system.<sup>41,42</sup> We demonstrate that melatonin prevented mitochondrial edema, cristae dilatation, high NADPH oxidase activity, and apoptosis (Figures 2 and 3). Several reports indicate that mitochondria are an essential target for melatonin protection. The mechanisms implicated include the preservation of function complex I and III, the inhibition of mitochondrial permeability transition pore opening, and cytochrome c release.<sup>43,44</sup> Melatonin enhances mitofusin-2 expression, which preserves the mitochondrial functional

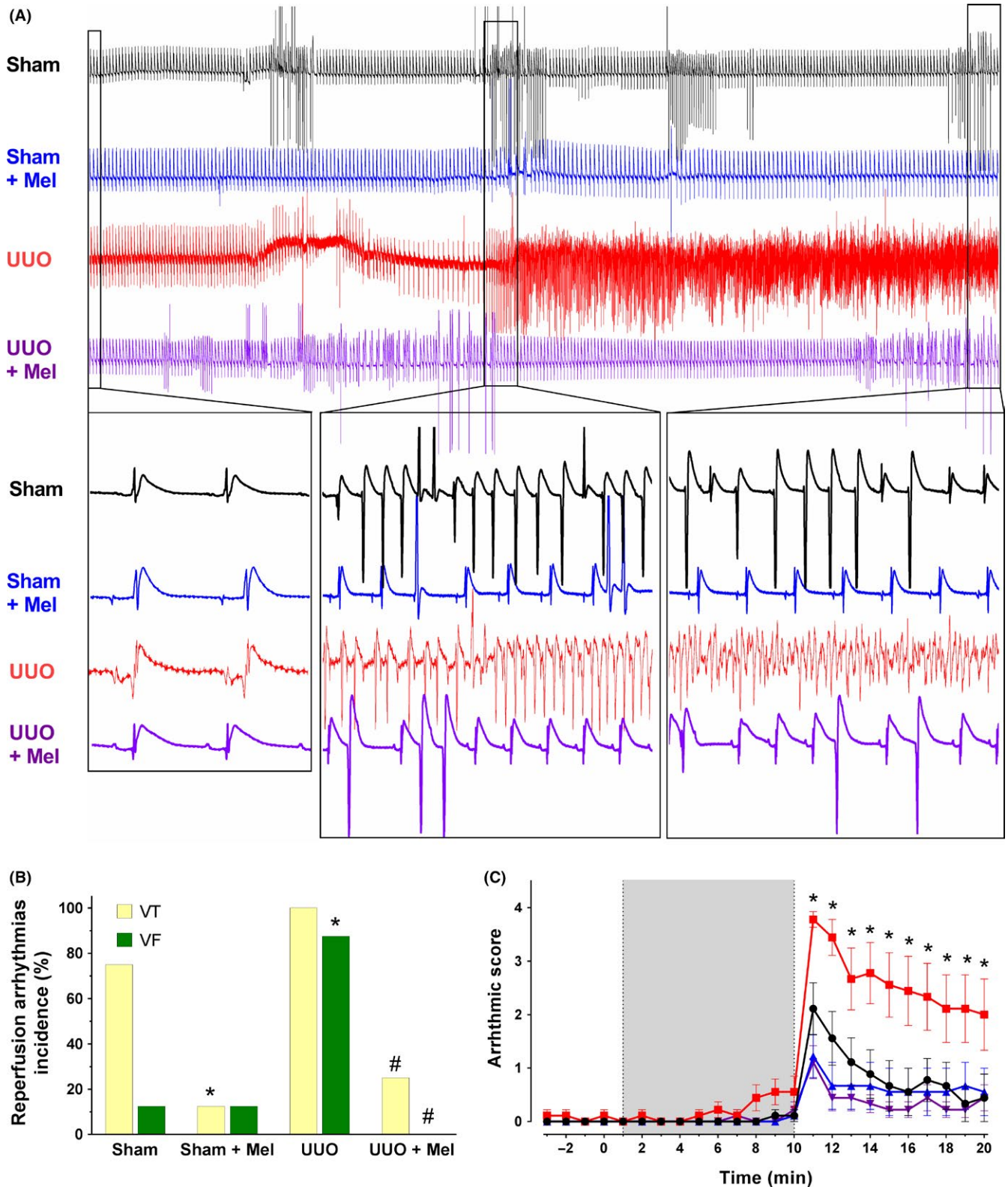


**FIGURE 9** Melatonin reduced reperfusion arrhythmias. A, Representative electrograms of the last 10 seconds of ischemia and the first 50 seconds of reperfusion from the 4 groups. For clarity, the lower insets show augmented time scales. The first inset corresponds to 0.5 seconds; the others correspond to 2 seconds. B, The incidence of reperfusion arrhythmias. Yellow and green bars indicate ventricular tachycardia (VT) and ventricular fibrillation (VF), respectively. C, The arrhythmic score observed minute-by-minute. \* $P < .05$  vs Sham; # $P < .05$  vs UVO

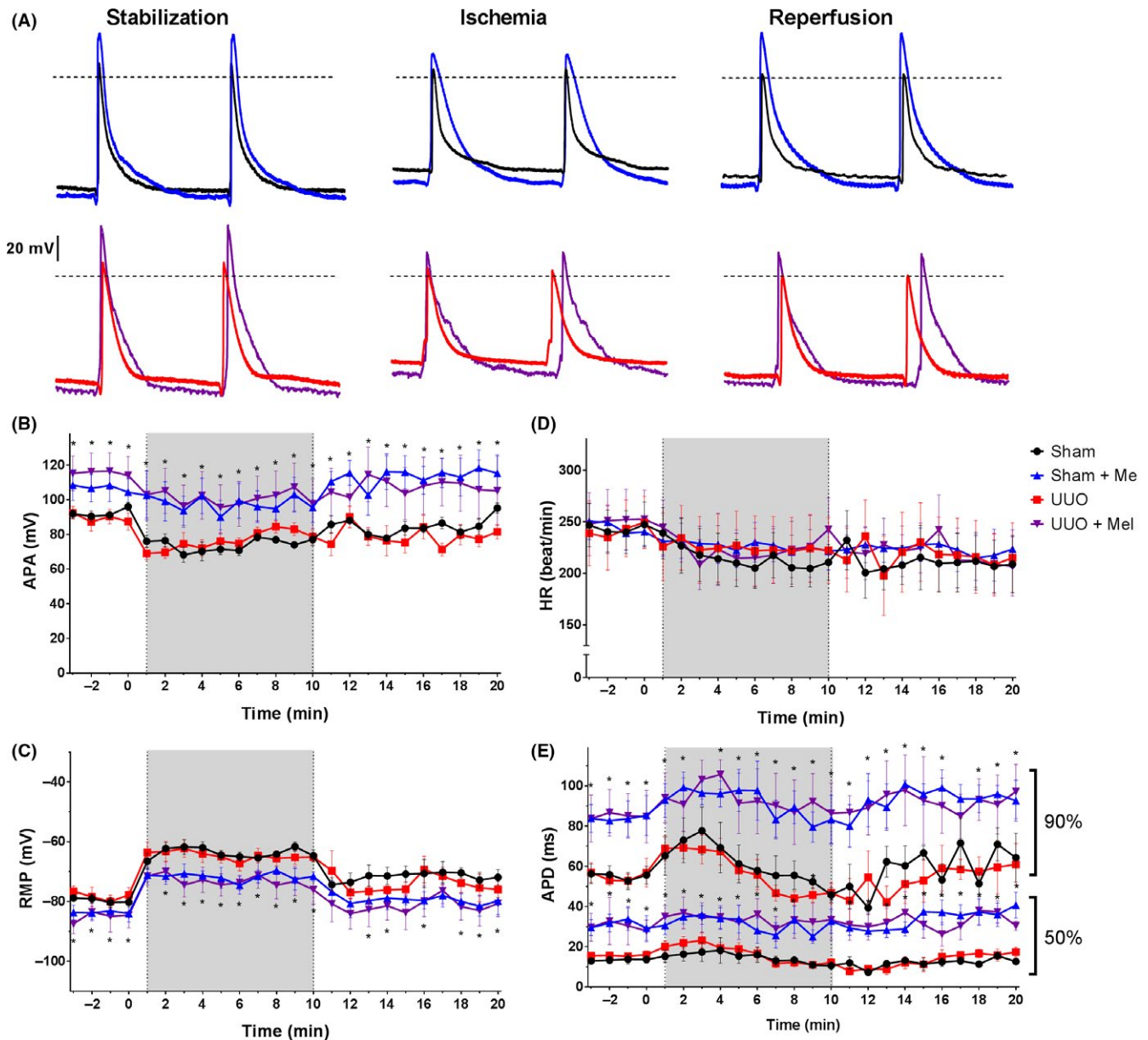


**FIGURE 10** Action potential characterization: Melatonin's effect. A, Representative traces of epicardial action potentials (500 ms each) from the experimental periods. The colors are coded black for Sham, blue for Sham + Mel, red for UUO, and violet for UUO + Mel. Horizontal dashed lines are traced at 0 mV. B, Action potential amplitude (APA) averaged values from each minute during the protocol. The gray area indicates the ischemic period. C, Resting membrane potential (RMP). D, Heart rate (HR). E, Action potential duration (APD): The four upper traces correspond to measures made at 90% of the repolarization and the 4 lower ones to duration at 50% of the repolarization  $*P < .01$  vs untreated groups

network and prevents apoptosis.<sup>44,45</sup> Yu et al reported that mitofusin-2 inhibits angiotensin II-induced myocardial hypertrophy.<sup>46</sup> In this sense, melatonin reduction of mitochondrial damage could be linked to  $AT_1$  down-regulation. Melatonin induction of Hsp70 supports an additional mechanism related to Tom70, a translocase of the outer mitochondrial membrane. Hsp70 interaction with Tom70 is essential for the initiation of the import process.<sup>47</sup> Relevant to our understanding, Tom70 regulates melatonin-induced protection against myocardial infarction, by breaking the cycle of mitochondrial impairment and ROS generation.<sup>48,49</sup> All these

data allow us to assume that melatonin induction of Hsp70 and reduction of  $AT_1$  are critical components of the cellular stress response.

Finally, and in parallel with the molecular and structural studies, it was of central interest to our study to evaluate the functionality of the heart. Thus, UUO increased vulnerability to suffering ventricular fibrillation during reperfusion (Figure 9). We attribute this arrhythmogenesis to the prooxidative and profibrotic changes that accompanied the increase in  $AT_1$  and the decrease in Hsp70. Myocardial oxidative stress—particularly in the mitochondria—and fibrosis

are well-known proarrhythmic substrates.<sup>50-52</sup> Free radicals act as triggers for the beginning of arrhythmic events. The persistence of high-frequency rhythms requires some reentrance.<sup>53</sup> Impaired conduction and action potential shortening (as shown in Figures 9 and 10) contribute to the complex reentrant mechanisms involved in ventricular fibrillation.

Melatonin protection against myocardial remodeling induced by UUO is one of the factors that protect against ventricular fibrillation. The increase in Hsp70 limits the deleterious AT<sub>1</sub> up-regulation and VDR down-regulation. Hsp70 also contributes to the antioxidant effect of melatonin, confirmed here by mitochondrial NADPH activity reduction. Moreover, action potential lengthening and hyperpolarization (shown in Figure 10) are reasonable contributors to the antiarrhythmic effect of melatonin. These changes are the first report of myocardial action potential modification by chronic melatonin administration. The melatonin receptors activate inward rectifier potassium currents that could explain the hyperpolarization.<sup>54</sup> The lengthening of the action potential corresponds with the inhibitory effect of melatonin against outward potassium currents, which are principally responsible for rat myocyte repolarization.<sup>55</sup> The attenuated response to ischemia-induced action potential shortening has been previously observed in our laboratory and agrees with the down-regulation of the volume-regulated chloride channels reported by Ben Soussia et al<sup>56</sup> The complex scenario of chronic melatonin administration's effects on ionic currents requires further investigation.

To conclude, in this article we explore the protective mechanisms of chronic melatonin treatment in kidney disease and cardiovascular complications. We focus our attention on the preventive effects of melatonin against disturbance in mitochondrial oxidant capacity, ultrastructure, and apoptosis. Additionally, melatonin protected from the proarrhythmic state associated with UUO. Our results suggest new mechanisms of renal and cardioprotection by melatonin. The modulation of AT<sub>1</sub> and VDR receptors linked to the increase in Hsp70 contribute to the effects of melatonin. Finally, we highlight the therapeutic potential of Mel against diseases associated with deleterious effects of increased AT<sub>1</sub> function.

## ACKNOWLEDGEMENT

The authors thank Bob Ritchie from Ponce Health Sciences University for his proofreading service and Adriana M. Carrión for her technical assistance.

## AUTHORS' CONTRIBUTION

N. J. Prado involved in the conception and design, acquisition of data, data analysis/interpretation, and drafting of the manuscript. M. Casarotto, J. P. Calvo, L. Mazzei, I. M. García, F. D. Cuello-Carrión, and M. W. Fornés involved in

the acquisition, analysis, and interpretation of data. L. Ferder involved in the design, data analysis, and interpretation. A. Z. Ponce Zumino, E. R. Diez, and W. Manucha involved in the conception, design, data acquisition, analysis and interpretation, financial support, and drafting of the manuscript. All the authors critically revised and approved the final manuscript.

## CONFLICT OF INTEREST

The author(s) declared no potential conflicts of interest with respect to the research, authorship, and/or publication of this article.

## ORCID

Emiliano Raúl Diez  <http://orcid.org/0000-0001-5163-3703>

## REFERENCES

1. Bonato FOB, Watanabe R, Lemos MM, Cassiolato JL, Wolf M, Canziani MEF. Asymptomatic ventricular arrhythmia and clinical outcomes in chronic kidney disease: a pilot study. *Cardiorenal Med.* 2016;7:66-73.
2. Daimee UA, Biton Y, Moss AJ, et al. Effect of cardiac resynchronization therapy on the risk of ventricular tachyarrhythmias in patients with chronic kidney disease. *Ann Noninvasive Electrocardiol.* 2017;22:e12404.
3. Franczyk-Skóra B, Gluba-Brzózka A, Wrancik JK, Banach M, Olszewski R, Rysz J. Sudden cardiac death in CKD patients. *Int Urol Nephrol.* 2015;47:971-982.
4. Pun PH. The interplay between CKD, sudden cardiac death, and ventricular arrhythmias. *Adv Chronic Kidney Dis.* 2014;21:480-488.
5. Reddan DN, Szczech L, Bhapkar MV, et al. Renal function, concomitant medication use and outcomes following acute coronary syndromes. *Nephrol Dial Transplant.* 2005;20:2105-2112.
6. Diez ER, Altamirano LB, García IM, et al. Heart remodeling and ischemia-reperfusion arrhythmias linked to myocardial vitamin D receptors deficiency in obstructive nephropathy are reversed by paricalcitol. *J Cardiovasc Pharmacol Ther.* 2015;20:211-220.
7. Poeggeler B, Reiter RJ, Tan D-X, Chen L-D, Manchester LC. Melatonin, hydroxyl radical-mediated oxidative damage, and aging: A hypothesis. *J Pineal Res.* 1993;14:151-168.
8. Rosen J, Than NN, Koch D, Poeggeler B, Laatsch H, Hardeland R. Interactions of melatonin and its metabolites with the ABTS cation radical: extension of the radical scavenger cascade and formation of a novel class of oxidation products, C2-substituted 3-indolinones. *J Pineal Res.* 2006;41:374-381.
9. Hardeland R, Tan D-X, Reiter RJ. Kynuramines, metabolites of melatonin and other indoles: the resurrection of an almost forgotten class of biogenic amines. *J Pineal Res.* 2009;47:109-126.
10. Ishigaki S, Ohashi N, Isobe S, et al. Impaired endogenous nighttime melatonin secretion relates to intrarenal renin-angiotensin system activation and renal damage in patients with chronic kidney disease. *Clin Exp Nephrol.* 2016;20:878-884.

11. Russcher M, Koch B, Nagtegaal E, van der Putten K, ter Wee P, Gaillard C. The role of melatonin treatment in chronic kidney disease. *Front Biosci (Landmark Ed)*. 2012;17:2644-2656.
12. Esposito T, Rendina D, Aloia A, et al. The melatonin receptor 1A (MTNR1A) gene is associated with recurrent and idiopathic calcium nephrolithiasis. *Nephrol Dial Transplant*. 2012;27:210-218.
13. Ozbek E, Ilbey YO, Ozbek M, Simsek A, Cekmen M, Somay A. Melatonin attenuates unilateral ureteral obstruction-induced renal injury by reducing oxidative stress, iNOS, MAPK, and NF- $\kappa$ B expression. *J Endourol*. 2009;23:1165-1173.
14. Xu W, Cai S-Y, Zhang Y, et al. Melatonin enhances thermotolerance by promoting cellular protein protection in tomato plants. *J Pineal Res*. 2016;61:457-469.
15. Tas U, Ogeturk M, Kuloglu T, et al. HSP70 immune reactivity and TUNEL positivity in the liver of toluene-inhaled and melatonin-treated rats. *Toxicol Ind Health*. 2013;29:514-522.
16. Madhu P, Reddy KP, Reddy PS. Role of melatonin in mitigating chemotherapy-induced testicular dysfunction in Wistar rats. *Drug Chem Toxicol*. 2016;39:137-146.
17. Cheung RTF, Tipoe GL, Tam S, Ma ESK, Zou LY, Chan PS. Preclinical evaluation of pharmacokinetics and safety of melatonin in propylene glycol for intravenous administration. *J Pineal Res*. 2006;41:337-343.
18. Diez ER, Renna NF, Prado NJ, et al. Melatonin, given at the time of reperfusion, prevents ventricular arrhythmias in isolated hearts from fructose-fed rats and spontaneously hypertensive rats. *J Pineal Res*. 2013;55:166-173.
19. Sezgin G, Oztürk G, Güney S, Sinanoğlu O, Tunçdemir M. Protective effect of melatonin and 1,25-dihydroxyvitamin D3 on renal ischemia-reperfusion injury in rats. *Ren Fail*. 2013;35:374-379.
20. Chua S, Lee F-Y, Chiang H-J, et al. The cardioprotective effect of melatonin and exendin-4 treatment in a rat model of cardiorenal syndrome. *J Pineal Res*. 2016;61:438-456.
21. Hruska KA, Guo G, Wozniak M, et al. Osteogenic protein-1 prevents renal fibrogenesis associated with ureteral obstruction. *Am J Physiol Renal Physiol*. 2000;279:F130-F143.
22. Morrissey J, Hruska K, Guo G, Wang S, Chen Q, Klahr S. Bone morphogenetic protein-7 improves renal fibrosis and accelerates the return of renal function. *J Am Soc Nephrol*. 2002;13(Suppl 1):S14-S21.
23. O'Beirne GB, Williams DC. The subcellular location in rat kidney of the peripheral benzodiazepine acceptor. *Eur J Biochem*. 1988;175:413-421.
24. García IM, Mazzei L, Benardón ME, et al. Caveolin-1-eNOS/Hsp70 interactions mediate rosuvastatin antifibrotic effects in neonatal obstructive nephropathy. *Nitric oxide Biol Chem*. 2012;27:95-105.
25. Gago FE, Tello OM, Diblasi AM, Ciocca DR. Integration of estrogen and progesterone receptors with pathological and molecular prognostic factors in breast cancer patients. *J Steroid Biochem Mol Biol*. 1998;67:431-437.
26. Ciocca DR, Cuello-Carrión FD, Natoli AL, Restall C, Anderson RL. Absence of caveolin-1 alters heat shock protein expression in spontaneous mammary tumors driven by Her-2/neu expression. *Histochem Cell Biol*. 2012;137:187-194.
27. Curtis MJ, Hearse DJ. Reperfusion-induced arrhythmias are critically dependent upon occluded zone size: relevance to the mechanism of arrhythmogenesis. *J Mol Cell Cardiol*. 1989;21:625-637.
28. Walker MJ, Curtis MJ, Hearse DJ, et al. The Lambeth Conventions: guidelines for the study of arrhythmias in ischaemia infarction, and reperfusion. *Cardiovasc Res*. 1988;22:447-455.
29. Curtis MJ, Walker MJ. Quantification of arrhythmias using scoring systems: an examination of seven scores in an in vivo model of regional myocardial ischaemia. *Cardiovasc Res*. 1988;22:656-665.
30. Hrenak J, Paulis L, Repova K, et al. Melatonin and renal protection: novel perspectives from animal experiments and human studies (review). *Curr Pharm Des*. 2015;21:936-949.
31. Egan Benova T, Szeiffova Bacova B, Viczenczova C, Diez E, Barancik M, Tribulova N. Protection of cardiac cell-to-cell coupling attenuate myocardial remodeling and proarrhythmia induced by hypertension. *Physiol Res*. 2016;65(Suppl 1):S29-S42.
32. Leja-Szpak A, Pierzchalski P, Goralska M, et al. Kynuramines induce overexpression of heat shock proteins in pancreatic cancer cells Via 5-hydroxytryptamine and MT1/MT2 receptors. *J Physiol Pharmacol*. 2015;66:711-718.
33. Bocanegra V, Manucha W, Peña MR, Cacciamani V, Vallés PG. Caveolin-1 and Hsp70 interaction in microdissected proximal tubules from spontaneously hypertensive rats as an effect of Losartan. *J Hypertens*. 2010;28:143-155.
34. García IM, Altamirano L, Mazzei L, et al. Vitamin D receptor-modulated Hsp70/AT1 expression may protect the kidneys of SHR at the structural and functional levels. *Cell Stress Chaperones*. 2014;19:479-491.
35. Wu S, Ren S, Chen H, Chun RF, Gacad MA, Adams JS. Intracellular vitamin D binding proteins: novel facilitators of vitamin D-directed transactivation. *Mol Endocrinol*. 2000;14:1387-1397.
36. He B, Zhao Y, Xu L, et al. The nuclear melatonin receptor ROR  $\alpha$  is a novel endogenous defender against myocardial ischemia/reperfusion injury. *J Pineal Res*. 2016;60:313-326.
37. Ellison TI, Eckert RL, MacDonald PN. Evidence for 1,25-dihydroxyvitamin D3-independent transactivation by the vitamin D receptor: uncoupling the receptor and ligand in keratinocytes. *J Biol Chem*. 2007;282:10953-10962.
38. Zittermann A. Vitamin D and disease prevention with special reference to cardiovascular disease. *Prog Biophys Mol Biol*. 2006;92:39-48.
39. Lutz W, Kohno K, Kumar R. The role of heat shock protein 70 in vitamin D receptor function. *Biochem Biophys Res Commun*. 2001;282:1211-1219.
40. Baltatu O, Afeche SC, José dos Santos SH, et al. Locally synthesized angiotensin modulates pineal melatonin generation. *J Neurochem*. 2002;80:328-334.
41. Baltatu OC, Amaral FG, Campos LA, Cipolla-Neto J. Melatonin, mitochondria and hypertension. *Cell Mol Life Sci*. 2017;74:3955-3964.
42. Ohashi N, Isobe S, Ishigaki S, Yasuda H. Circadian rhythm of blood pressure and the renin-angiotensin system in the kidney. *Hypertens Res*. 2017;40:413-422.
43. Petrosillo G, Di Venosa N, Pistolese M, et al. Protective effect of melatonin against mitochondrial dysfunction associated with cardiac ischemia- reperfusion: role of cardiolipin. *FASEB J*. 2006;20:269-276.
44. Stacchiotti A, Favero G, Giugno L, et al. Mitochondrial and metabolic dysfunction in renal convoluted tubules of obese

- mice: protective role of melatonin. Ashton N, ed. *PLoS ONE*. 2014;9:e111141.
45. Kawalec P. Disease activity, quality of life and indirect costs associated with ulcerative colitis in Poland. *Value Heal*. 2016;19:A585.
  46. Yu H, Guo Y, Mi L, Wang X, Li L, Gao W. Mitofusin 2 inhibits angiotensin II-induced myocardial hypertrophy. *J Cardiovasc Pharmacol Ther*. 2011;16:205-211.
  47. Fan ACY, Young JC. Function of cytosolic chaperones in Tom70-mediated mitochondrial import. *Protein Pept Lett*. 2011;18:122-131.
  48. Pei H-F, Hou J-N, Wei F-P, et al. Melatonin attenuates post-myocardial infarction injury via increasing Tom70 expression. *J Pineal Res*. 2017;62:e12371.
  49. Ma Z, Xin Z, Di W, et al. Melatonin and mitochondrial function during ischemia/reperfusion injury. *Cell Mol Life Sci*. 2017;74:3989-3998.
  50. Brown DA, O'Rourke B. Cardiac mitochondria and arrhythmias. *Cardiovasc Res*. 2010;88:241-249.
  51. Sovari AA, Rutledge CA, Jeong EM, et al. Mitochondria oxidative stress, connexin43 remodeling, and sudden arrhythmic death. *Circ Arrhythmia Electrophysiol*. 2013;6:623-631.
  52. Montaigne D, Maréchal X, Lacroix D, Staels B. From cardiac mitochondrial dysfunction to clinical arrhythmias. *Int J Cardiol*. 2015;184:597-599.
  53. Jalife J. Ventricular fibrillation: mechanisms of initiation and maintenance. *Annu Rev Physiol*. 2000;62:25-50.
  54. Nelson CS, Marino JL, Allen CN. Melatonin receptors activate heteromeric G-protein coupled Kir3 channels. *NeuroReport*. 1996;7:717-720.
  55. Hou SW, Zheng P, Sun FY. Melatonin inhibits outward delayed rectifier potassium currents in hippocampal CA1 pyramidal neuron via intracellular indole-related domains. *J Pineal Res*. 2004;36:242-249.
  56. Ben SI, Mies F, Naeije R, Shlyonsky V. Melatonin down-regulates volume-sensitive chloride channels in fibroblasts. *Pflugers Arch Eur J Physiol*. 2012;464:273-285.

## SUPPORTING INFORMATION

Additional supporting information may be found online in the Supporting Information section at the end of the article.

**How to cite this article:** Prado NJ, Casarotto M, Calvo JP, et al. Antiarrhythmic effect linked to melatonin cardiorenal protection involves AT<sub>1</sub> reduction and Hsp70-VDR increase. *J Pineal Res*. 2018;e12513. <https://doi.org/10.1111/jpi.12513>